Biochimica et Biophysica Acta 1857 (2016) 772–781

Contents lists available at ScienceDirect

Biochimica et Biophysica Acta

journal homepage: www.elsevier.com/locate/bbabio

The switching mechanism of the mitochondrial ADP/ATP carrier explored by free-energy landscapes

Adriana Pietropaolo [a,*], Ciro Leonardo Pierri [b], Ferdinando Palmieri [b], Martin Klingenberg [c,*]

[a] Dipartimento di Scienze della Salute, Università di Catanzaro, Viale Europa, 88100 Catanzaro, Italy
[b] Department of Biosciences, Biotechnologies and Biopharmaceutics, University of Bari, Via E. Orabona 4, 70125 Bari, Italy
[c] Institut für Physiologische Chemie, Schillerstr.44, 80336 München, Germany

ARTICLE INFO

Article history:
Received 28 October 2015
Received in revised form 1 February 2016
Accepted 8 February 2016
Available online 10 February 2016

Keywords:
AAC
Conformational states
Mitochondria
Mitochondrial carrier
Molecular dynamics
Transport mechanism

ABSTRACT

The ADP/ATP carrier (AAC) of mitochondria has been an early example for elucidating the transport mechanism alternating between the external (c-) and internal (m-) states (M. Klingenberg, Biochim. Biophys. Acta 1778 (2008) 1978–2021). An atomic resolution crystal structure of AAC is available only for the c-state featuring a three repeat transmembrane domain structure. Modeling of transport mechanism remained hypothetical for want of an atomic structure of the m-state. Previous molecular dynamics studies simulated the binding of ADP or ATP to the AAC remaining in the c-state. Here, a full description of the AAC switching from the c- to the m-state is reported using well-tempered metadynamics simulations. Free-energy landscapes of the entire translocation from the c- to the m-state, based on the gyration radii of the c- and m-gates and of the center of mass, were generated. The simulations revealed three free-energy basins attributed to the c-, intermediate- and m-states separated by activation barriers. These simulations were performed with the empty and with the ADP- and ATP-loaded AAC as well as with the poorly transported AMP and guanine nucleotides, showing in the free energy landscapes that ADP and ATP lowered the activation free-energy barriers more than the other substrates. Upon binding AMP and guanine nucleotides a deeper free-energy level stabilized the intermediate-state of the AAC2 hampering the transition to the m-state. The structures of the substrate binding sites in the different states are described producing a full picture of the translocation events in the AAC.

1. Introduction

ATP generated by oxidative phosphorylation in mitochondria is exported into the cytosol of eukaryotic cells across the inner mitochondrial membrane by a one to one exchange of ATP against ADP. Since the translocated ionization species are ATP^{4-} and ADP^{3-}, the exchange is electrogenic and driven by the high membrane potential of the inner mitochondrial membrane. ATP and ADP are preferred to AMP and to nucleotides with other bases [1]. The ADP/ATP transport is catalyzed by the ADP/ATP carrier (AAC), the prototype of the mitochondrial solute carrier family (SLC25) that transports a variety of nucleotides, carboxylates, amino acids, coenzymes and inorganic anions, and whose loss-of-function has been found to be responsible of many diseases [2–4]. The ADP/ATP transport is distinguished by highly specific and efficient inhibitors, atractyloside (ATR) and its derivatives from plants and bongkrekic acid (BKA) from bacteria [1,5]. The structures of the hydrophilic ATR group and of the hydrophobic BKA are very different, in line with the findings that ATR inhibits only from the outside and BKA from the matrix side. By studying the binding of ADP and ATP in combination with ATR and BKA to AAC the switching of the binding center from the c-side to the m-side of the inner membrane was demonstrated as a first example of the alternate site (single binding center gated pore) mechanism [6,7]. With ATR the AAC was fixed in the c-state and with BKA in the m-state. The transition between these states requires ADP or ATP. This substrate dependent catalysis led to the "induced transition fit" concept postulating that the optimum fit of the substrate to the carrier is reached in the transition state [8]. The AAC from bovine heart was isolated in a native stable state in complex with carboxyatractyloside (CAT) [9], whereas the isolated AAC-BKA complex was highly labile [10]. The primary structure [11] suggested that AAC consists of six transmembrane helices arranged in a three repeat structure [12]. A crystal structure of the bovine AAC1-CAT complex at 2.2 Å resolution confirmed the three-fold repeated structure arranged around a translocation path along a threefold axis [13,14] representing AAC in the c-state with the channel wide open to the c-side. The putative binding site with three positively charged residues is near the center of the membrane. At the bottom of the binding cavity three tight ion pairs around the central path represent the closed m-gate in the c-state. Near the c-side three loose ion pairs are suggested to form the wide open c-gate [15,16]. The structure provides a basis for elucidating the

Abbreviations: AAC, ADP/ATP carrier; CAT, carboxyatractyloside; ATR, atractyloside; BKA, bongkrekic acid.

* Corresponding authors.
E-mail addresses: apietropaolo@unicz.it (A. Pietropaolo), klingenberg@med.uni-muenchen.de (M. Klingenberg).

http://dx.doi.org/10.1016/j.bbabio.2016.02.006
0005-2728/

mechanism of ADP and ATP translocation, involving the structural changes on substrate binding and the gating at both sides of the channel. Earlier molecular dynamics simulations [17–20] of the bovine AAC1 elucidated energetic and structural features of ADP and ATP binding, producing insights into the forces which guide the substrate to the binding site. These studies were necessarily limited to the stage where the carrier fluctuated around the c-state conformations, before entering the subsequent conformations leading to the intermediate- and the m-state.

Here we have employed free-energy simulations in the framework of well-tempered [21] metadynamics [22] to follow the transition all the way from the c- to the m-state. We used well-tempered metadynamics instead of molecular dynamics because it is an extremely efficient and highly accurate method for the prediction of structural changes in proteins associated with the changes of the free-energy levels [23–25]. The gyration radii of the three key regions of AAC2, namely the c-gate, the center of mass and the m-gate, were chosen as the most appropriate collective variables (CVs) [23–28] to describe the opening and closing of the AAC2 and the conformational switching associated to substrate transport. Free-energy landscapes were reconstructed using the gyration radii of the c- and m-gates revealing three free-energy basins corresponding to the c-, m- and intermediate-states. The free-energies of the transitions as well as the structural changes of the human AAC2 were determined for the empty and nucleotide loaded AAC2. The factors enabling ADP and ATP and preventing AMP and guanine nucleotides to be transported were elucidated. Different free-energy levels of the intermediate-states and of the surrounding activation barriers were found to be critical factors for transport. Thus we could generate a probabilistic path of the AAC from the initial c-state conformation to the final m-state conformation aiming at disclosing the switching mechanism from the c-state to the m-state through quantitative free-energy estimates.

2. Materials and methods

2.1. Simulation of the conformation changes

The conformational changes that AAC2 undergoes during the transition from the c-state to the m-state were evaluated from the free-energy landscapes of AAC2 in the presence and absence of adenine and guanine nucleotides. For studying the switching mechanism from the c-state to the m-state, the collective variables which best reflect the protein conformation changes of the transition between the translocation states are the gyration radii calculated in three specific regions of the carrier, namely the c-gate ($\rho_{c\text{-}gate}$), the center of mass (ρ_{center}) and the m-gate ($\rho_{m\text{-}gate}$) (Fig. S1 of the Supplementary material). $\rho_{c\text{-}gate}$ is defined by the C_α coordinates of the residues F12, F89, D93, K96, L117, F192, D196, K199, T214, L288, D292 and K295 of the c-gate [15,16] and the aromatic belt [29]. ρ_{center} is defined by the C_α coordinates of the residues K23, R80, L128, G183, G225 and R280 of the substrate binding site [30–32]. $\rho_{m\text{-}gate}$ is defined by the C_α coordinates of the residues P28, E30, K33, G73, P133, D135, R138, G176, P230, D232, R235 and G273 of the m-gate [13] and the PG-level 2 [33,34]. All these residues were chosen based on their implication in the carrier translocation pathway as elucidated in the literature [13,15,16,29,30–32,35,36].

The radius of gyration, ρ, is defined using the standard formula shown in Eq. (1)–(2):

$$\varrho_{j=}\left(\frac{\sum_i^n m_{i,j}\left|\mathbf{r}_{i,j}-\mathbf{r}_{COM,j}\right|^2}{\sum_i^n m_{i,j}}\right)^{\frac{1}{2}} \quad (1)$$

$$\mathbf{r}_{COM,j}=\frac{\sum_i^n \mathbf{r}_{i,j}m_{i,j}}{\sum_i^n m_{i,j}} \quad (2)$$

where $r_{i,j}$ are the coordinates of the atom i listed above, j identifies the three circular sections of the carrier describing the gyration radii (i.e. $\rho_{c\text{-}gate}$, ρ_{center}, $\rho_{m\text{-}gate}$) and $r_{COM,j}$ are the coordinates of the centers of mass for the three circular sections. Any change of the three gyration radii reflects the opening and closing of the c- and m-gates during the switching from the c- to the m-state as a consequence of the substrate binding and translocation. Given that the values of ρ_{center} did not significantly differ during the entire course of the free-energy simulations, the free-energy landscapes reported in this manuscript were reconstructed by using the gyration radii of the c- and m-gates.

2.2. Simulation details

Given that the human AAC2 shares more than 90% of the identical residues with the crystallized bovine AAC1, the initial structure of human AAC2 was obtained through comparative modeling [37,38] by using the bovine AAC1 structure (PDB code 1OKC) [13] as a template. The C-terminal portion ^{295}KKYT^{298} of AAC2 not represented in the crystallized bovine AAC1 was subsequently added at the C-terminus after an initial equilibration of the segment by using the available crystallized structures of yeast AAC2 (pdb code 4C9H) and AAC3 (pdb code 4C9Q) as a template-driving structures [39]. The generated 3D model was inserted in a thermalized palmitoyl-oleyl-phosphatidylcholine (POPC) bilayer consisting of 110 lipid units solvated in 9156 water molecules. The net excess charge of the empty AAC2 was neutralized adding 17 chloride counterions. The system was equilibrated with 10 ns of MD simulation. In addition, 10 ns of steered molecular dynamics (SMD) [40] were initially run in order to sample initial m-state conformations.

1 μs of preliminary simulations of well-tempered [21] metadynamics [22] were run for AAC2 in order to check whether the three gyration radii were suitable collective variables for reconstructing the switching mechanism from the c-state to the m-state. Moreover, the inter- and intra-repeat distances were monitored in the course of free-energy simulations. Multiple walkers [41] were added to the free energy simulations at the tightly closed c-state conformation displaying fully formed inter-repeat salt-bridges of the m-gate (K96-D196; K199-D292; D93-K295) and at the open m-state conformations displaying completely broken inter-repeat salt-bridges of the m-gate (E30-R138; K33-R232; D135-R235). The "Multiple walker" technique ensures the contribution of different conformations constituting local free-energy minima on the translocation pathway. This allows an accurate free-energy estimate since any dependence on starting artifacts, that can arise starting from a unique conformation, is removed. Fig. S2 of the Supplementary material reports the variations of the three gyration radii, $\rho_{c\text{-}gate}$, ρ_{center} and $\rho_{m\text{-}gate}$ as a function of the preliminary well-tempered metadynamics simulation for AAC2 in the absence of substrate. Thereafter, we run seven sets of well-tempered [21] metadynamics [22] (each 0.2 μs long) for AAC2 bound to ATP, ADP, AMP, GTP, GDP or GMP as well as for the empty AAC2 always using the three gyration radii as collective variables, in order to estimate the free-energy landscape of AAC2 switching from the c-state to the m-state and its variation upon nucleotide binding. To run well-tempered metadynamics for nucleotide-bound AAC2 the three free-energy basins, obtained from the initial 1 μs-long simulation for the empty AAC2 and representing the c-state, the intermediate-state and the m-state of the empty AAC2, were used. The nucleotides were inserted in the c-state, in the intermediate-state and in the m-state obtained by the preliminary empty AAC2 free-energy simulations, using the position close to Y195 and Y191, close to K23, R80, R280, R236 and close to G183, Y187, I184, S228 and G225. The net excess charge of AAC2 was neutralized by 13 Cl^- counterions in the presence of ATP and GTP, 14 Cl^- counterions in the presence of ADP and GDP, and 15 Cl^- counterions in the presence of AMP and GMP. Two quartic repulsive walls were placed at appropriate place to confine each nucleotide inside the AAC2 and avoid its exiting from the carrier. The first repulsive wall was placed in a space defined by the C_α coordinates of residues F12, F89, D93, K96, L117, F192, D196,

K199, T214, L288, D292 and K295 (at the level of the c-gate and the aromatic belt), and the second in a place defined by the C_α coordinates of residues P28, E30, K33, G73, P133, D135, R138, G176, P230, D232, R235 and G273 (between the binding site area and the m-gate). Multiple walkers [41] were added for each simulation to accelerate the free-energy convergence. The continuous mutual feedback on the free-energy computed for each conformation ensured to obtain a unique absolute free-energy minimum for each AAC2 state.

In order to assess the free-energy convergence we checked if the free-energy differences between the c-state and the m-state reached a constant value. The free-energy convergence profile is reported in Fig. S3 of the Supplementary material. Moreover, the standard error of the free-energy differences was estimated using the method of Tiwary and Parrinello [42]. For all the free-energy simulations that had been run, gaussians with a height of 0.2 kcal/mol were deposited at 1 ps time interval and with a bias factor equal to 10. NVT ensemble with a temperature of 300 K was enforced using a Langevin thermostat as implemented in the NAMD 2.9 molecular dynamics code [43]. AMBER99SB potential [44] was used for AAC2 and chlorine ions, the CHARMM force field for the POPC membrane [45] and the TIP3P potential [46] for water molecules. The parameters of Meagher et al. [47] were used for all the nucleotides. NAMD2.9 code [43] was used throughout the simulation together with the PLUMED1.3 plugin for metadynamics [48]. Periodic boundary conditions were applied. Electrostatic interactions were calculated using the Particle Mesh Ewald method [49]. The time-step was set to 2 fs. The SHAKE algorithm [50] was applied to fix all bond lengths.

The conformation states of AAC2 reported in this paper were selected among those present in each of the three basins of attraction of the free energy minima ascribed to each state. First, we clustered the conformations belonging to the three deepest free-energy minima. Among the clustered conformations we chose the conformations based on their ion-pair distances at the level of the c-gate and of the m-gate, whose ion pair distances are widely accepted to be involved in the AAC translocation pathway [13,15,16,33,34,39]. In particular, we selected the c-state among all the conformations belonging to the c-basin, by choosing the state with the shortest ion pairs among the residues of the m-gate and with the highest ion pairs among the residues of the c-gate (Table S1 of the Supplementary material). Similarly, for the m-state we selected the conformation, among those belonging to the m-basin, with the shortest ion pairs detectable among the residues of the c-gate and with the highest ion pairs detectable among the residues of the m-gate (Table S1 of the Supplementary material). For the intermediate- (closed) state we selected the conformation, among those belonging to the intermediate state basin, with the shortest ion pairs detectable among the residues of both the c-gate and the m-gate (Table S1 of the Supplementary material).

3. Results

3.1. The free energy as a guide for the gating mechanism of AAC2

The free-energy landscape of AAC2 in the absence of substrate was reconstructed with the two gyration radii of the AAC2 describing the c-gate and the m-gate as reaction coordinates (Fig. 1a and Fig. S1 of the Supplementary material). The free-energy surface showed a deep free-energy minimum with a stepwise connection to an intermediate free-energy minimum. An activation barrier of 10 kcal/mol high, centered at $\rho_{m\text{-}gate} = 12.1$ Å, $\rho_{c\text{-}gate} = 14.7$ Å, separated the deep free-energy minimum from a second broad free-energy minimum. This broad minimum was less stable by 3.8 kcal/mol than the deepest one, whereas the intermediate free-energy basin was less stable by 6.0 kcal/mol than the deepest free-energy minimum. In agreement with expectations, the gyration radii $\rho_{c\text{-}gate}$ and $\rho_{m\text{-}gate}$ change in opposite direction along the transition path of the free-energy landscape. The deepest free-energy basin centered at $\rho_{m\text{-}gate} = 9.7$ Å, $\rho_{c\text{-}gate} = 14.4$ Å identified the c-state conformation (Fig. 1a and Table S2 of the Supplementary material). The intermediate free-energy basin was centered at $\rho_{m\text{-}gate} = 11.0$ Å, $\rho_{c\text{-}gate} = 13.5$ Å. This free-energy basin corresponded to the stepwise closing of the c-gate and the opening start of the m-gate (Fig. 1a and Table S2 of the Supplementary material). The final broad free-energy basin centered at $\rho_{m\text{-}gate} = 12.7$ Å, $\rho_{c\text{-}gate} = 12.0$ Å identified a conformation approaching the m-state (Fig. 1a and Table S2).

Upon binding ATP, ADP or AMP, the free-energy landscape of AAC2 showed striking differences with that of AAC2 in the absence of substrates. Furthermore, the free-energy profiles of ATP-, ADP- and AMP-bound AAC2s were distinctly different from each other. In the presence of ATP the m-state was nearly as stable as the c-state. Again high values of $\rho_{c\text{-}gate}$ and low values of $\rho_{m\text{-}gate}$ were observed in the c- state and vice versa in the assigned m-state: the c-state minimum is at $\rho_{m\text{-}gate} = 9.6$ Å, $\rho_{c\text{-}gate} = 14.9$ Å and the m-state minimum is at $\rho_{m\text{-}gate} = 13.7$ Å, $\rho_{c\text{-}gate} = 11.8$ Å. An activation barrier of 10 kcal/mol centered at $\rho_{m\text{-}gate} = 11.8$ Å, $\rho_{c\text{-}gate} = 11.5$ Å separated the c-state from the m-state (Fig. 1b). The intermediate free-energy basin was less stable by 6.1 kcal/mol than the deepest free-energy minimum. Remarkably, in the presence of ATP i) the m-state and the c-state free-energy difference decreased to 1.4 kcal/mol as compared with 3.8 kcal/mol of the AAC2 in the absence of substrate (Table 1) and ii) the c-state conformation in the presence of ATP was more open towards the c-gate ($\rho_{m\text{-}gate} = 9.6$ Å, $\rho_{c\text{-}gate} = 14.9$ Å) than with AAC2 in the absence of substrate ($\rho_{m\text{-}gate} = 9.7$ Å, $\rho_{c\text{-}gate} = 14.4$ Å) (Fig. 1a and b and Table S2 of the Supplementary material). Furthermore, ATP markedly stabilized the c- and m-conformations of AAC2 as shown by their narrower free-energy basins compared to those of the c- and m-states of the empty AAC2 (Fig. 1a and b).

Upon binding of ADP, the c-state basin was centered at $\rho_{m\text{-}gate} = 9.8$ Å, $\rho_{c\text{-}gate} = 14.5$ Å, and the m-state basin at $\rho_{m\text{-}gate} = 13.5$ Å, $\rho_{c\text{-}gate} = 12.0$ Å. They were connected through an intermediate basin (Fig. 1c). Due to the increased depth of the intermediate basin located at $\rho_{m\text{-}gate} = 11.3$ Å, $\rho_{c\text{-}gate} = 12.8$ Å, a high activation barrier ($\rho_{m\text{-}gate} = 11.8$ Å, $\rho_{c\text{-}gate} = 11.7$ Å) of 8 kcal/mol (Table 1) separated the intermediate- and the m-state. In comparison with the situation in which ATP was bound to AAC2, the m-state and the c-state free-energy difference of the ADP-bound AAC2 increased to 2.2 kcal/mol, indicating that the m-state of the ADP-bound AAC2 was more stable than that of AAC2 in the absence of substrate and less stable than that of the ATP-bound AAC2 (Table 1).

Upon binding of AMP, the free-energy profile became diffuse with three deep free-energy basins (Fig. 1d). In particular, the c-state was split in two minima, the deepest one was centered at $\rho_{m\text{-}gate} = 9.2$ Å, $\rho_{c\text{-}gate} = 13.4$ Å (Table S2 of the Supplementary material). The second minimum at $\rho_{m\text{-}gate} = 9.7$ Å, $\rho_{c\text{-}gate} = 16.4$ Å was less stable than the first by 3 kcal/mol (Fig. 1d). The free-energy level of the intermediate basin centered at $\rho_{m\text{-}gate} = 11.0$ Å, $\rho_{c\text{-}gate} = 12.6$ Å was fairly close to the free-energy level of the c-state (Fig. 1d and Table S2). Two activation barriers centered at $\rho_{m\text{-}gate} = 10.5$ Å, $\rho_{c\text{-}gate} = 14.3$ Å and at $\rho_{m\text{-}gate} = 11.8$ Å, $\rho_{c\text{-}gate} = 13.0$ Å separated the c-state from the m-state (Fig. 1d, Table 1). The m-state basin was also split in different minima, with the deepest one centered at $\rho_{m\text{-}gate} = 12.5$ Å, $\rho_{c\text{-}gate} = 11.9$ Å (Fig. 1d and Table S2 of the Supplementary material). Intriguingly, at variance with the situation in which ATP or ADP were bound to AAC2 i) the free-energy difference between the c-state and m-state increased to

Fig. 1. Free-energy profile of the AAC2 transition between c- and m-state, calculated by well-tempered metadynamics on the basis of the AAC crystal structure. Free-energy profiles are shown in the absence of substrate a) and in the presence of adenine nucleotides b)–d) as a function of the m-gate and c-gate gyration radii. The c-state, the intermediate-state and the m-state basins are highlighted by C, I and M labels, respectively. The free-energy scale is in kcal/mol. Red arrows indicate the directionality of the AAC2 transition pathway. The origin of the arrows and the two arrow-heads indicate the location of the c-, intermediate-, and m-state free-energy minima selected within the three basins, according to the maximum opening/closing of the c- and m-gate ion pairs. Further details on the selection of the conformations are reported in Materials and methods.

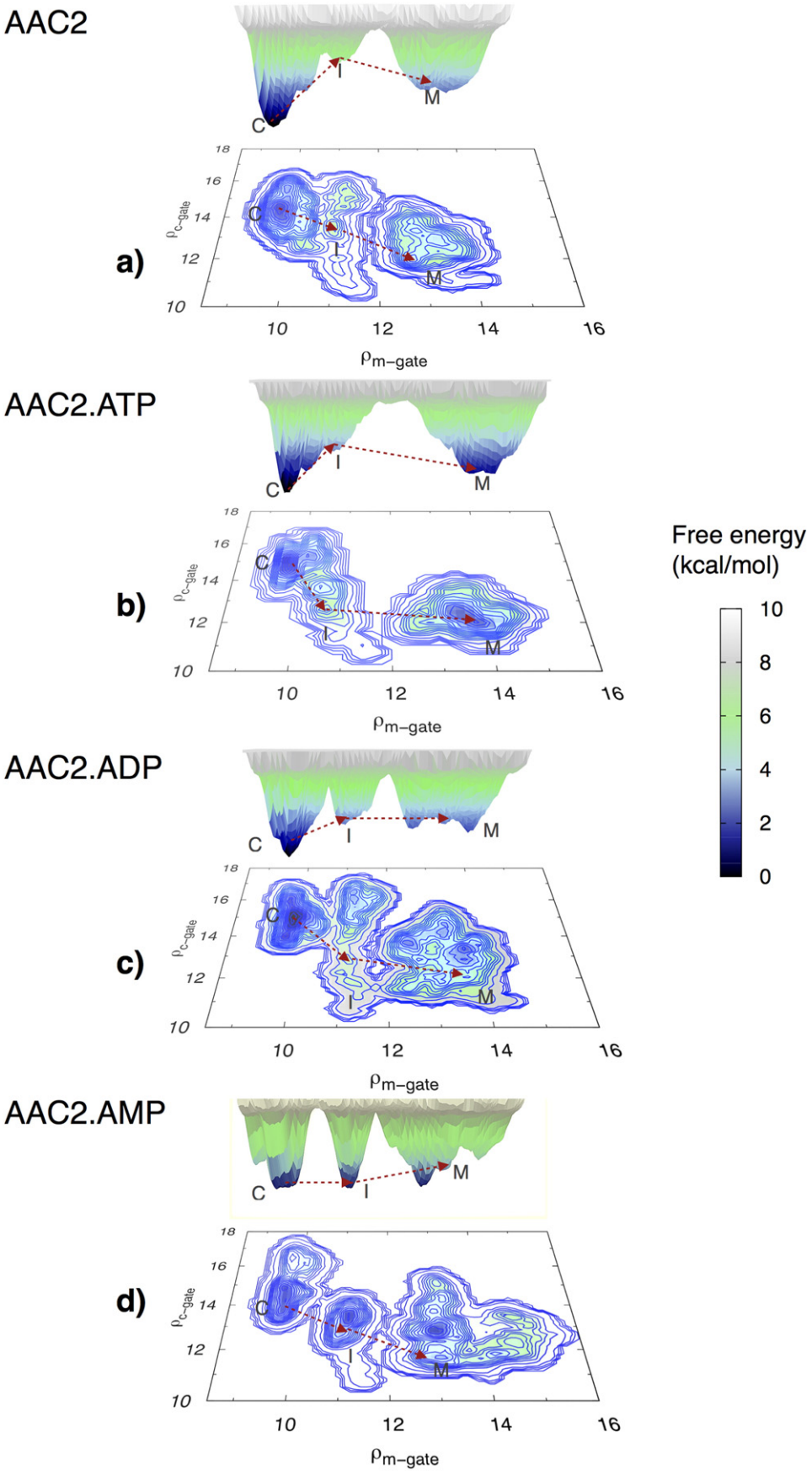
AAC2
C
I
M
a)
ρ_{c-gate}
ρ_{m-gate}
AAC2.ATP
b)
AAC2.ADP
c)
AAC2.AMP
d)
Free energy
(kcal/mol)
10
8
6
4
2
0

Table 1
Free-energy differences (kcal/mol) between the c-state and the m-state ($\Delta G^\circ_m - \Delta G^\circ_c$) and between the c-state and the intermediate-state ($\Delta G^\circ_i - \Delta G^\circ_c$). Activation barriers ($\Delta G^*$) for the transition from the c-state to the m-state are also reported. The standard error of the free-energy differences was estimated to be about 0.6 kcal/mol.

	$\Delta G^\circ_m - \Delta G^\circ_c$ (kcal/mol)	$\Delta G^\circ_i - \Delta G^\circ_c$ (kcal/mol)	ΔG^* (kcal/mol)
AAC2	3.8	6.0	10.0
AAC2.ATP	1.4	6.1	10.0
AAC2.ADP	2.2	4.0	8.0
AAC2.AMP	4.7	1.7	7.4; 6.3
AAC2.GTP	4.5	2.6	10.0; 7.5
AAC2.GDP	4.2	2.3	6.1; 5.5
AAC2.GMP	4.7	2.2	6.8; 6.4

4.7 kcal/mol (Table 1), a value even higher than that of AAC2 in the absence of substrate (3.8 kcal/mol), ii) the intermediate-state displayed a stable free-energy minimum and iii) two high activation barriers separated the c-state from the m-state basins. This pattern was also observed when AAC2 was bound by guanine nucleotides, namely GTP, GDP and GMP (Fig. 2, Table 1 and Table S2 of the Supplementary material). The free-energy landscapes appeared even more diffuse featuring two high free-energy barriers and a high stable intermediate basin. These findings show that the probability that AAC2 bound to guanine nucleotides reaches the m-state conformation is quite low, in agreement with the results reported in Table 1.

3.2. Structural basis for the gating mechanism

3.2.1. The c-state

In the preceding section, the free-energy levels served as a guide to define the critical functional states of the AAC during the translocation. The underlying structure changes in these states will be elucidated in this section. A critical parameter for the characterization of the c- and m- states is the opening/closing of the gates formed by the inter-repeat ion pairs, shown in Fig. 3. The distances in the ion pairs reflect quantitatively the opening/closing of the gates. The c-state conformation of AAC2 (Fig. 3) in the absence of substrate associated with the free-energy minimum of Fig. 1a displays an open c-gate and a nearly closed m-gate. The binding of the translocated substrates ATP and ADP caused a very slight c-gate opening in the c-state conformation (Fig. 3 and Table S2 of the Supplementary material). The binding of AMP induced more closed conformations of the c- and m-gates than in the absence of substrates as well as in the presence of the other nucleotides. Furthermore, AMP induced a second set of open conformations of the c-gate, which are less stable by 3 kcal/mol (Fig. 1d). Interestingly, upon binding of guanine nucleotides to AAC2 the c-states observed along the free-energy simulations were different in the shape of their conformations (Fig. S4 of the Supplementary material) compared to those observed upon binding of ATP and ADP, in line with the fact that GTP, GDP, GMP are not translocated by AAC2.

3.2.2. The intermediate-state

The intermediate-state conformation of AAC2 corresponding to the free-energy minimum in the absence of substrate (Fig. 1a) showed an m-gate slightly more open than in the c-state conformation (Fig. 3). In contrast, the c-gate was slightly more closed than in the c-state conformation (Table S2 of the Supplementary material). In the presence of ATP, the m-gate in the intermediate-state was more open than that observed in the c-state, whereas the c-gate was narrower than that observed in the c-state of the empty AAC2 and in the c-state of the ATP-bound AAC2 (Table S2 of the Supplementary material). In the presence of ADP, the m-gate of the intermediate-state was more open than in the presence of ATP and the c-gate had the same inter-repeat ion pair distances in the presence of ATP in the same state (Table S2 of the Supplementary material). Comparing the adenine and guanine nucleotides, the intermediate-state conformations observed in the presence of each of the three guanine ligands had a more open c-gate (Table S2 of the Supplementary material).

3.2.3. The m-state

In the absence of substrate, the m-gate of AAC2 derived from the free-energy simulations (Fig. 1a) was more closed than in the presence of the active substrates (Table S2 of the Supplementary material). The free-energy simulation derived m-state conformations exhibit an opening of the m-gate only upon the binding of ATP and ADP and a concurrent closing of the c-gate only upon binding of ATP (Fig. 3). Intriguingly and confirming the expectations, with the poorly transported AMP the m-state conformations of AAC2 were similar to those of the empty AAC2 (Table S2, Fig. S4 of the Supplementary material). A similar behavior was observed upon binding of guanine nucleotides (Table S2, Fig. S4).

3.3. Binding site regions in the c-, intermediate- and m-states

In the conformational landscape of the AAC2 c-state, all three adenine nucleotides were bound to a similar set of residues (Fig. 4, Table S3 of the Supplementary material). In particular, ATP formed salt bridges with K96 and K199, ADP with K92 and K96, AMP with K92 and K199 (Table S3 of the Supplementary material). Furthermore, ATP and ADP formed π-stacking interactions with Y195, F192 and Y191 of the aromatic belt [29] and H-bond interactions with N116, N88 (only ADP) and R188 in the substrate binding area [30–32]. GTP and GDP appeared to be more mobile, establishing interactions with residues located between the c-gate area and the substrate binding area, whereas GMP bound similarly to AMP (Table S3 of the Supplementary material). In the intermediate-state and in the m-state of AAC2, ATP, ADP and AMP formed salt bridges with positively charged residues (R80, R280, K33 and R236) (Tables S4–S5 of the Supplementary material). Furthermore, in the m-state ATP and ADP (and to a lower extent AMP) formed π-stacking interactions with Y187 and salt bridges with R188 near the c-gate as well as with Q37 in the m-gate area (Fig. 4). It is noteworthy that the interactions between AAC2 and guanine nucleotides were markedly different from those found with ATP or ADP (Tables S3–S5 of the Supplementary material). For example, they often involved flexible residues (as Gly or Ala) indicating a lack of specificity in the binding of guanine ligands to AAC2. This seems to be another factor why AAC2 transports ATP or ADP much more efficiently than guanine nucleotides.

4. Discussion

The AAC has been a leading target for addressing the transport mechanism of solute carriers, due to the existence of unique natural and highly specific inhibitors which fix the carrier either in the c- or m-state of the translocation cycle [1]. This enabled not only the isolation of an intact carrier for the first time but also to recognize the existence of two translocation states in the isolated form. The atomic crystal structure of the AAC–carboxyatractyloside complex [13] finally solidified in atomic detail the three repeat structure, originally proposed on the basis of the sequence [11,12] and chemical and mutational probing [1]. The structure with the striking threefold salt bridges and mobility-conferring residues called for models of the transport mechanism [2, 13,16,33]. With more advanced variants of molecular dynamics, the binding steps of the substrate ADP were simulated [17,18]. Thus it was demonstrated how ADP was guided into the open funnel of AAC to the binding site by the electrostatic forces exerted by the excess positive residues on the negatively charged ADP^{3-}. These simulations were necessarily confined to the c-state conformations of the AAC.

In this work, free-energy simulations in the framework of well-tempered metadynamics [21,22] enabled us to reconstruct the free-energy surface during the substrate translocation using the two

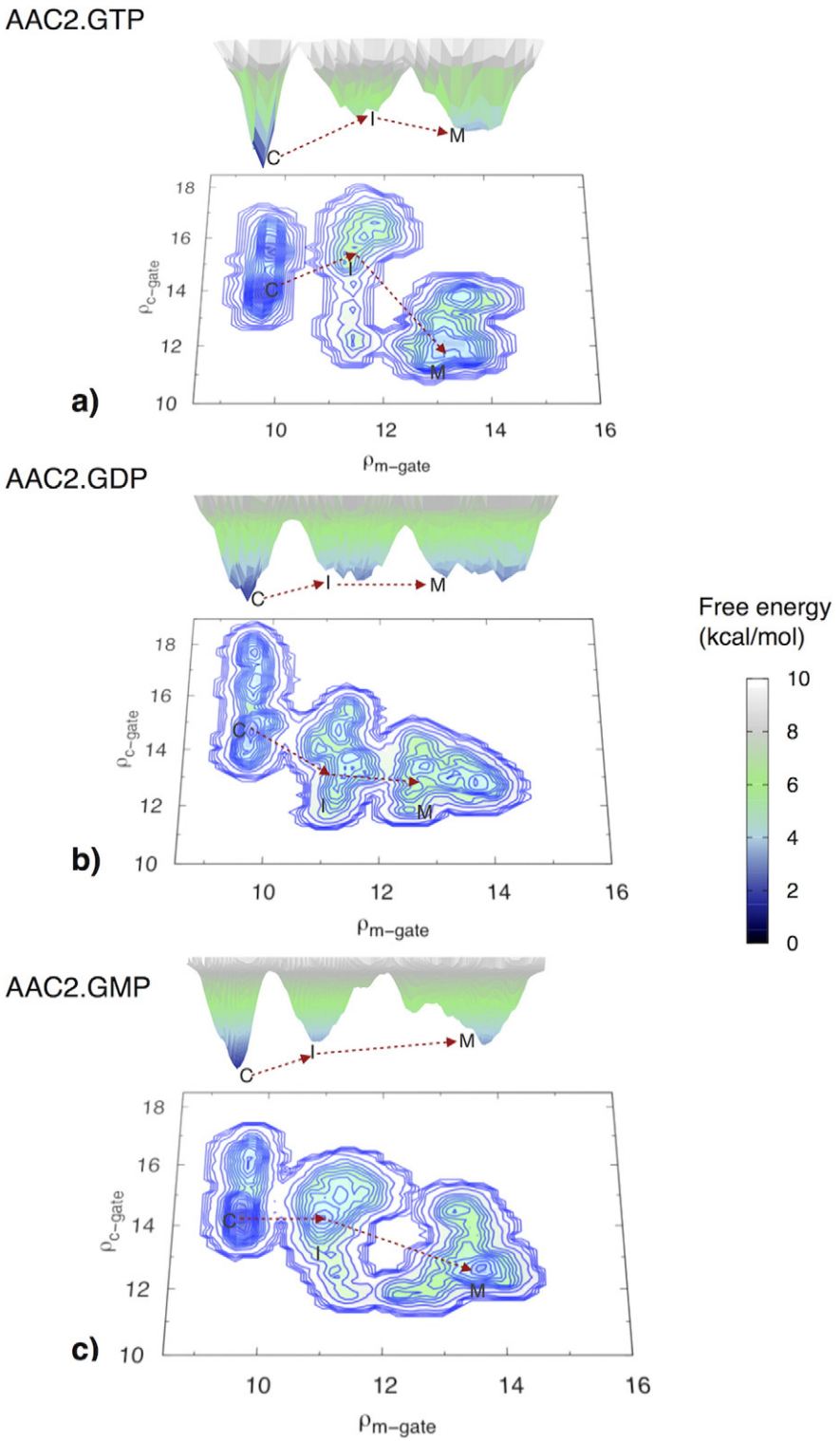

Fig. 2. Free-energy profile of the AAC2 transition between c- and m-state, calculated by well-tempered metadynamics on the basis of the AAC crystal structure. Free-energy profiles are shown in the presence of guanine nucleotides namely GTP a), GDP b) and GMP c) as a function of the m-gate and c-gate gyration radii. The c-state, the intermediate-state and the m-state basins are highlighted by C, I and M labels, respectively. The free-energy scale is in kcal/mol. Red arrows indicate the directionality of the AAC2 transition pathway. The origin of the arrows and the two arrow-heads indicate the location of the c-, intermediate-, and m-state free-energy minima selected within the three basins, according to the maximum opening/closing of the c- and m-gate ion pairs. Further details on the selection of the conformations are reported in Materials and methods.

gyration radii of the c- and m-gate as Cartesian coordinates. In this way a complete free-energy surface experienced by the carrier going from the initial c-state to the final m-state was obtained and the conformational changes that AAC undergoes during the entire translocation process could be traced. The simulations were performed with the empty AAC2, with ATP- or ADP-bound AAC2 and also with poorly transported nucleotides as a control to elucidate the transport facilitating factors. Thus at variance with classical molecular dynamics well-tempered metadynamics has enabled us to observe on extended time-scales the conformational changes of the AAC2 translocation.

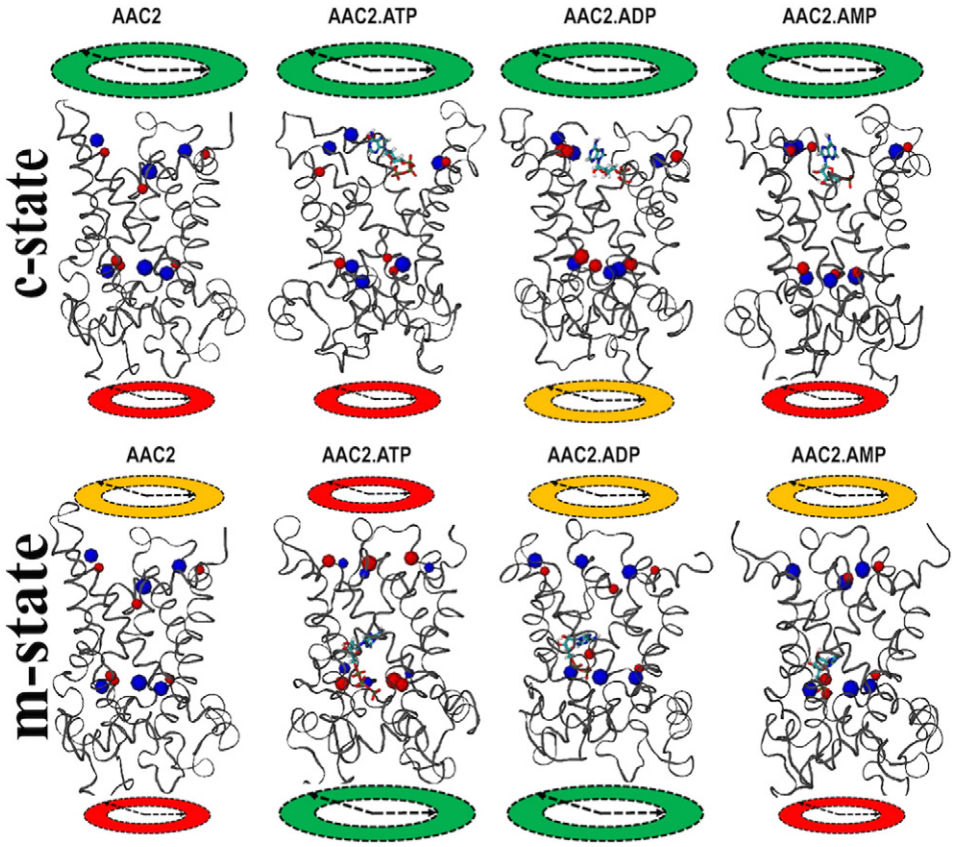

Fig. 3. The conformations of the c-state and m-state of AAC2 obtained from free-energy simulations in the presence and absence of adenine nucleotides. The conformations of the AAC2 correspond to the c-, intermediate- and m-state selected from the free-energy landscapes as indicated in Materials and methods. The upper and lower circles refer to the c-gate and m-gate, respectively. The gate opening is highlighted in green, the gate closing in red and a halfway state in yellow. The extent of gate opening/closing is indicated by the size of the circles. Blue beads represent basic amino acids involved in the m-gate ion-pairs (bottom-half of each structure) or in the c-gate ion pairs (top-half of each structure). Red beads represent acidic amino acids involved in the m-gate ion-pairs (bottom-half of each structure) or in the c-gate ion pairs (top-half of each structure).

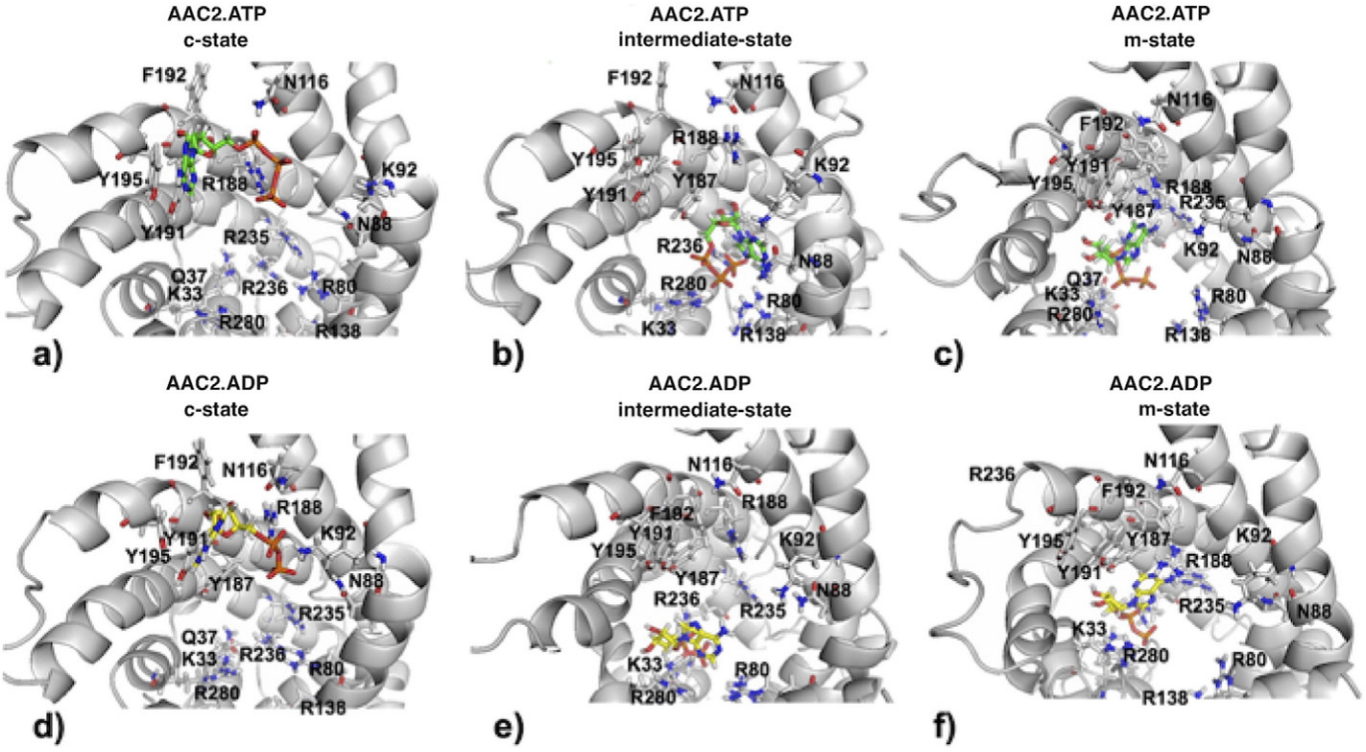

Fig. 4. The binding sites of AAC2 for ATP (a–c) and ADP (d–f) in the c-state, in the intermediate-state and in the m-state. ATP carbon backbone is shown in green and ADP carbon backbone is shown in yellow. Oxygen is shown in red, nitrogen in blue and phosphorus in brown. Further details on the binding modes are reported in the Supplementary material.

The free-energy simulations provide evidence for the existence of two distinct conformation states of AAC, in agreement with the previous biochemical evidence for the c- and m-states [1,6,7]. In addition, the simulations identified intermediate conformations of AAC2 related to the transition state of transport. Two major free-energy basins near the extremes of the gyration radii were observed. Within the deepest free-energy basin a large $\rho_{c\text{-}gate}$ reflected the c-gate opening and thus the c-state, whereas within the other free energy basin a large value of $\rho_{m\text{-}gate}$ indicated the m-gate opening and thus the m-state. Less well defined free-energy basins existed between the c- and m-states and corresponded to the intermediate-state. Within these states, equal values of $\rho_{c\text{-}gate}$ and $\rho_{m\text{-}gate}$ represented an intermediate state closed on both the cytosolic and matrix sides. The free-energy differences concerning the transition of AAC2 from the c-state to the intermediate state and from the intermediate state to the m-state, listed in Table 1, are correlated to the probability of transition of AAC between the three states in the presence or absence of nucleotides.

Our free-energy simulations also provide an insight in two important issues concerning the function of AAC2, i.e. how the transition of AAC between the c- and m-state is facilitated by the substrates ADP and ATP and how ADP and ATP are transported about 10 to 20 faster than AMP, GDP and GTP. Free AAC2 needs to overcome an activation barrier approaching 10 kcal/mol (Table 1), indicating a low probability of AAC2 switching without ATP and ADP (Fig. 5). Interestingly, previous adaptive bias force simulations [17] calculated that a free-energy difference of 10 kcal/mol was generated upon binding of ADP to its binding site, indicating that the substrate binding allows the carrier to acquire the activation free-energy needed for the gating, i.e. switching from the c-state to the m-state. Notably, the free energy simulations reported herein calculated an activation barrier of 10 kcal/mol for the AAC2 in the absence of substrate and in the presence of ATP, whereas of 8 kcal/mol in the presence of ADP. Therefore the intermediate-state with ADP is stabilized 2 kcal/mol more than that in the presence of ATP or in the absence of a substrate (Table 1).

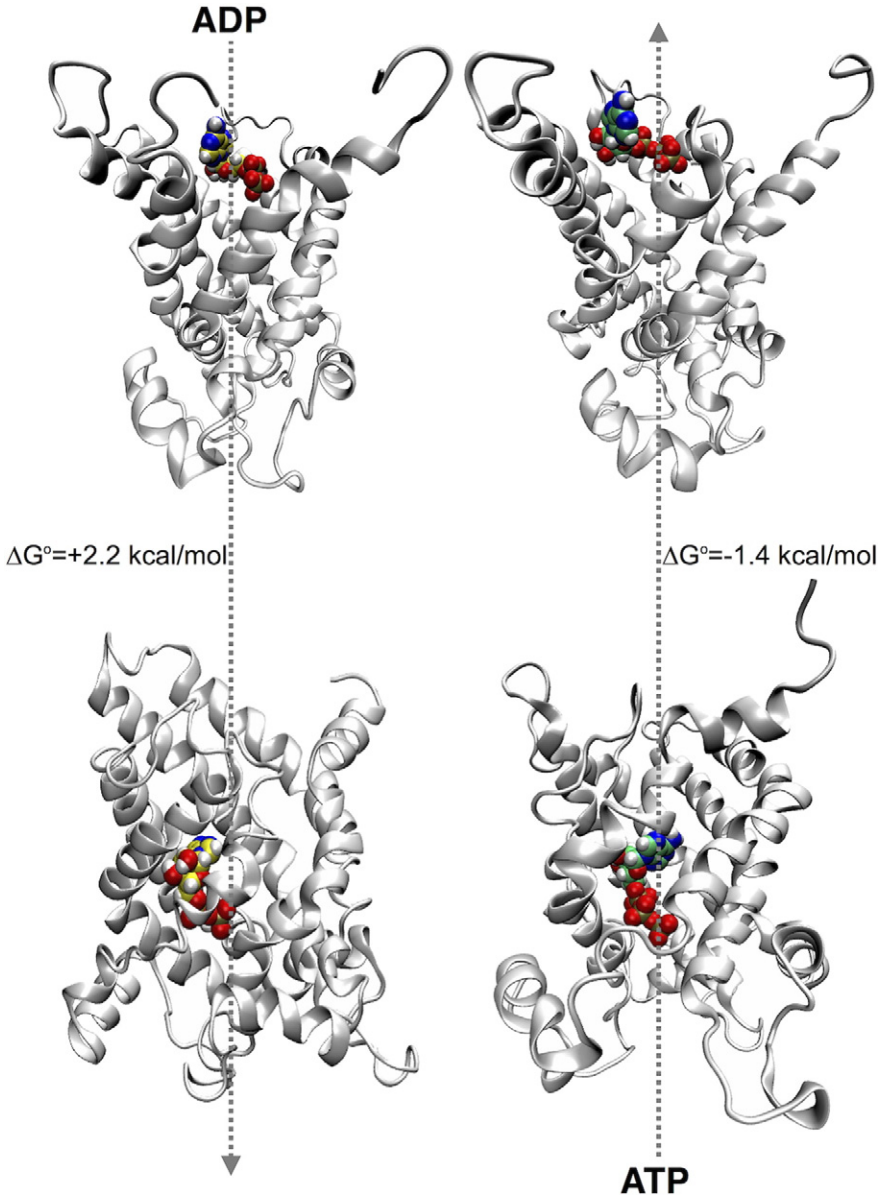

Fig. 5. The gating mechanism of AAC2 upon binding ADP and ATP nucleotides. Free-energy differences between the final and initial states (m-state and c-state for ADP and c-state and m-state for ATP) occurring during the translocation are reported in kcal/mol. The arrow-heads indicate the direction of the translocation pathway in the physiological hetero-exchange between external ADP and internal ATP.

In addition, our results are in agreement with the "induced transition fit" theorem of carrier-catalyzed transport [8] which postulates that the fit between the carrier binding site and the substrate is suboptimal in the c- and m-states and reaches an optimum fit in the intermediate-state. The free-energy released from the optimum fit is consumed by the free-energy needed to facilitate the conformation changes of the gating process. Indeed, the shallow intermediate free-energy basins and the resulting high free-energy level of the central intermediate-state, observed only with the active substrates ADP and ATP, are in agreement with the postulated compensation of the high free-energy produced by the intermediate-state binding and the energy used by the conformational rearrangements. The resulting labile state characterizes an efficient transition-state for the active substrates. The data reported in Tables Tables S3–S5 of the Supplementary material give supporting evidence for this view as the number of AAC2 residues distant to less than 4 Å from ATP and ADP and thus involved in the binding is much greater in the intermediate- (closed) state than in the c-state. Conversely, inactive substrates should be less able to induce a transition-state conformation due to an imperfect fit. In accordance with the simulated free-energy profiles, this results in a less compensated and deeper intermediate free-energy basin.

The free-energy profiles also explain why AMP and guanine nucleotides are not or poorly transported. In other words, how can it be explained that with AMP and guanine nucleotides, AAC may not easily reach the m-state? Discrete free-energy minima for the c-state and the m-state with only one sharp activation barrier were observed with the empty AAC2 and on binding ATP and, to a lower extent, ADP (Fig. 1 a–c). By contrast, AMP- and guanine nucleotides-bound AAC2s displayed free-energy landscapes featuring less distinct minima (Figs. 1d and 2). Two sharp and high barriers in the free-energy profiles, as shown in Figs. 1d and 2 and Table 1, have to be overcome. Further, the free-energy profiles showed less stable minima than with the ATP or ADP (Figs. 1 and 2). Finally, the free-energy basins of the intermediate-state were distinctly broader and deeper with the inactive than with the active nucleotides (Figs. 1 and 2). Only in the presence of ATP and ADP the radius of gyration in the m-gate was as high as 13.7 Å and 13.5 Å, respectively, and in the c-gate was as low as 11.8 Å and 12.0 Å, respectively (Table S2 of the Supplementary material). This observation indicates that AAC upon binding poorly transported substrates cannot escape easily from the intermediate-state, once the carrier approaching this state has fallen into the energy trap. Conversely, the active substrates (ADP and ATP) suppress this trap by allowing the transition to proceed to the m-state and avoiding the stabilization of the intermediate-state. This interpretation is further supported in quantitative terms by the estimation of the free-energy differences between the intermediate- and the c-state which are smaller in the presence of inactive substrates compared to those in the presence of active substrates or without any substrate (Table 1). In a recent publication devoted to the substrate specificity of AAC (the bovine AAC1) (Mifsud et al. [51]), the specificity was determined not only by transport measurements in reconstituted vesicles but also by simulating the nucleotide binding with molecular dynamics. In particular, in the MD simulations, by comparing adenine and guanine nucleotides on a time scale of at least 15 ns, it was found that the anchoring of the phosphate moieties of both adenine and guanine nucleotides was equally fast, whereas the anchoring of the guanosine moiety was 2 to 4 times statistically slower than that of the adenosine moiety. These results are in essential agreement with those obtained by our different metadynamics approach. It should be noted that the published results refer to nucleotide binding to AAC in the c-state, whereas in our work binding differences between adenine and guanine nucleotides were found in the c-state as well as in the intermediate- and m-state (Tables S3–S5 of the Supplementary material).

In conclusion, well-tempered metadynamics simulations provide the entire cycle of the conformation changes and energetic profiles of AAC going from the c- to the m-state. The free-energy changes explain how ADP and ATP binding facilitates the translocational transition of AAC. Further they show that the energetic profiles of binding other ligands such as AMP and the three guanine nucleotides are unfavorable to induce their transport by the AAC.

Transparency document

The Transparency document associated with this article can be found, in online version.

Acknowledgments

ISCRA resources supported the results achieved on the FERMI machine based in Italy. The Data Center ReCaS Bc^{2}S (Bari Computer Center for Science) is acknowledged for computational time provided.

Appendix A. Supplementary data

Supplementary data to this article including the coordinates of AAC2 in the presence and absence of adenine and guanine nucleotides in the c-, intermediate- and m-states can be found online in the Supplementary content. Supplementary data associated with this article can be found in the online version, at doi: 10.1016/j.bbabio.2016.02.006.

References

[1] M. Klingenberg, The ADP and ATP transport in mitochondria and its carrier, Biochim. Biophys. Acta 1778 (2008) 1978–2021.
[2] F. Palmieri, The mitochondrial transporter family SLC25: identification, properties and physiopathology, Mol. Asp. Med. 34 (2013) 465–484.
[3] F. Palmieri, Mitochondrial transporters of the SLC25 family and associated diseases: a review, J. Inherit. Metab. Dis. 37 (2014) 565–575.
[4] Y. Kishita, A. Pajak, N.A. Bolar, C.M.T. Marobbio, C. Maffezzini, D.V. Miniero, M. Monné, M. Kohda, H. Stranneheim, K. Murayama, K. Naess, N. Lesko, H. Bruhn, A. Mourier, R. Wibom, I. Nennesmo, A. Jespers, P. Govaert, A. Ohtake, L. Van Laer, B.L. Loeys, C. Freyer, F. Palmieri, A. Wredenberg, Y. Okazaki, A. Wedell, Intra-mitochondrial methylation deficiency due to mutations in SLC25A26, Am. J. Hum. Genet. 97 (2015) 1–8http://dx.doi.org/10.1016/j.ajhg.2015.09.013.
[5] P.V. Vignais, M.R. Blac, F. Boulay, F. Brandolin, G.J.M. Lanquin, in: G. Benga (Ed.), Molecular Aspects of Structure–Function Relationships in Mitochondrial Adenine Nucleotide Carrier in Structure and Properties of Cell Membranes, 2, CRC Press, Boca Raton, Florida 1985, pp. 139–179.
[6] M. Klingenberg, in: A.N. Martonosi (Ed.), The ADP/ATP Carrier in Mitochondrial Membranes, in the Enzymes of Biological Membranes: Membrane Transport, 3, Plenum Publishing Corp., New York, NY 1976, pp. 383–438.
[7] M. Klingenberg, The ADP/ATP shuttle of the mitochondrion, TIBS 4 (1979) 249–252.
[8] M. Klingenberg, Ligand–protein interaction in biomembrane carriers. The induced transition fit of transport catalysis, Biochemistry 44 (2005) 8563–8570.
[9] P. Riccio, B. Scherer, M. Klingenberg, Isolation of a new atractyloside type compound, FEBS Lett. 31 (1973) 11–14.
[10] H. Aquila, W. Eiermann, W. Babel, M. Klingenberg, Isolation of the ADP/ATP translocator from beef heart mitochondria as the bongkrekate-protein complex, Eur. J. Biochem. 85 (1978) 549–560.
[11] H. Aquila, D. Misra, M. Eulitz, M. Klingenberg, Complete amino acid sequence of the ADP/ATP carrier from beef heart mitochondria, Hoppe Seylers Z. Physiol. Chem. 363 (1982) 345–349.
[12] M. Saraste, J.E. Walker, Internal sequence repeats and the path of polypeptide in mitochondrial ADP/ATP translocase, FEBS Lett. 144 (1982) 250–254.
[13] E. Pebay-Peyroula, C. Dahout-Gonzalez, R. Kahn, V. Trézéguet, G.J. Lauquin, G. Brandolin, Structure of mitochondrial ADP/ATP carrier in complex with carboxyatractyloside, Nature 426 (2003) 39–44.
[14] H. Nury, C. Dahout-Gonzalez, V. Trézéguet, G.J. Lauquin, G. Brandolin, E. Pebay-Peyroula, Relations between structure and function of the mitochondrial ADP/ATP carrier, Annu. Rev. Biochem. 75 (2006) 713–741.
[15] A.J. Robinson, C. Overy, E.R. Kunji, The mechanism of transport by mitochondrial carriers based on analysis of symmetry, Proc. Natl. Acad. Sci. U. S. A. 105 (2008) 17766–17771.
[16] M.S. King, M. Kerr, P.G. Crichton, R. Springett, E.R. Kunji, Formation of a cytoplasmic salt bridge network in the matrix state is a fundamental step in the transport mechanism of the mitochondrial ADP/ATP carrier, Biochim. Biophys. Acta 1857 (2016) 14–22.
[17] F. Dehez, E. Pebay-Peyroula, C. Chipot, Binding of ADP in the mitochondrial ADP/ATP carrier is driven by an electrostatic funnel, J. Am. Chem. Soc. 130 (2008) 12725–12733.
[18] Y. Wang, E. Tajkhorshid, Electrostatic funneling of sub-strate in mitochondrial inner membrane carriers, Proc. Natl. Acad. Sci. U. S. A. 105 (2008) 9598–9603.

[19] M. Falconi, G. Chillemi, D. Di Marino, I. D'Annessa, B. Morozzo della Rocca, L. Palmieri, A. Desideri, Structural dynamics of the mitochondrial ADP/ATP carrier revealed by molecular dynamics simulation studies, Proteins 65 (2006) 681–691.
[20] D. Di Marino, F. Oteri, B. Morozzo Della Rocca, G. Chillemi, M. Falconi, ADP/ATP mitochondrial carrier MD simulations to shed light on the structural-dynamical events that, after an additional mutation, restore the function in a pathological single mutant, J. Struct. Biol. 172 (2010) 225–232.
[21] A. Barducci, G. Bussi, M. Parrinello, Well-tempered metadynamics: a smoothly converging and tunable free-energy method, Phys. Rev. Lett. 100 (2008) 020603.
[22] A. Laio, M. Parrinello, Escaping free-energy minima, Proc. Natl. Acad. Sci. U. S. A. 99 (2002) 12562–12566.
[23] A. Laio, F.L. Gervasio, Metadynamics: a method to simulate rare events and reconstruct the free energy in biophysics, chemistry and material science, Rep. Prog. Phys. 71 (2008) 1–22, 126601.
[24] G. Bussi, D. Branduardi, Free-energy calculations with metadynamics: theory and practice, Wiley Rev. Comput. Chem. 28 (2015) 1–49.
[25] S. Zheng, J. Pfaendtner, Enhanced sampling of chemical and biochemical reactions with metadynamics, J. Mol. Simul. 41 (2015) 55–72.
[26] A. Pietropaolo, T. Nakano, Molecular mechanism of poly-acrylate helix sense switching across its free energy landscape, J. Am. Chem. Soc. 135 (2013) 5509–5512.
[27] A. Pietropaolo, D. Branduardi, M. Bonomi, M. Parrinello, A chirality-based metrics for free-energy calculations in biomolecular systems, J. Comput. Chem. 32 (2011) 2627–2637.
[28] A. Pietropaolo, Y. Wang, T. Nakano, Predicting the switchable screw sense in fluorene-based polymers, Angew. Chem. Int. Ed. 23 (2015) 2688–2692.
[29] C.L. Pierri, F. Palmieri, A. De Grassi, Single-nucleotide evolution quantifies the importance of each site along the structure of mitochondrial carriers, Cell. Mol. Life Sci. 71 (2014) 349–364.
[30] A.J. Robinson, E.R.S. Kunji, Mitochondrial carriers in the cytoplasmic state have a common substrate binding site, Proc. Natl. Acad. Sci. U. S. A. 103 (2006) 2617–2622.
[31] C.M.T. Marobbio, G. Giannuzzi, E. Paradies, C.L. Pierri, F. Palmieri, alpha-Isopropylmalate, a leucine biosynthesis intermediate in yeast, is transported by the mitochondrial oxalacetate carrier, J. Biol. Chem. 283 (2008) 28445–28453.
[32] M. Monné, D.V. Miniero, L. Daddabbo, A.J. Robinson, E.R. Kunji, F. Palmieri, Substrate specificity of the two mitochondrial ornithine carriers can be swapped by single mutation in substrate binding site, J. Biol. Chem. 287 (2012) 7925–7934.
[33] F. Palmieri, C.L. Pierri, Structure and function of mitochondrial carriers — role of the transmembrane helix P and G residues in the gating and transport mechanism, FEBS Lett. 584 (2010) 1931–1939.
[34] F. Palmieri, C.L. Pierri, Mitochondrial metabolite transport, Essays Biochem. 47 (2010) 37–52.
[35] A.R. Cappello, R. Curcio, V.D. Miniero, I. Stipani, A.J. Robinson, E.R. Kunji, F. Palmieri, Functional and structural role of amino acid residues in the even-numbered transmembrane α-helices of the bovine mitochondrial oxoglutarate carrier, J. Mol. Biol. 363 (2006) 51–62.
[36] A.R. Cappello, R. Curcio, V.D. Miniero, I. Stipani, A.J. Robinson, E.R. Kunji, F. Palmieri, Functional and structural role of amino acid residues in the odd-numbered transmembrane α-helices of the bovine mitochondrial oxoglutarate carrier, J. Mol. Biol. 369 (2007) 400–412.
[37] N. Eswar, B. Webb, M.A. Marti-Renom, M.S. Madhusudhan, D. Eramian, S. Min-yi, U. Pieper, A. Sali, Current Protocols in Bioinformatics, John Wiley & Sons, Inc., 2006 5.6.1–5.6.30 (Supplement 15).
[38] C.L. Pierri, G. Parisi, V. Porcelli, Computational approaches for protein function prediction: a combined strategy from multi-ple sequence alignment to molecular docking-based virtual screen-ing, Biochim. Biophys. Acta 1804 (2010) 1695–1712.
[39] J.J. Ruprecht, A.M. Hellawell, M. Harding, P.G. Crichton, A.J. McCoy, E.R. Kunji, Structures of yeast mitochondrial ADP/ATP carriers support a domain-based alternating-access transport mechanism, Proc. Natl. Acad. Sci. U. S. A. 111 (2014) E426–E434.
[40] P.E. Marszalek, H. Lu, H. Li, M. Carrion-Vazquez, A.F. Oberhauser, K. Schulten, J.M. Fernandez, Mechanical unfolding intermediates in titin modules, Nature 402 (1999) 100–103.
[41] P. Raiteri, A. Laio, F.L. Gervasio, C. Micheletti, M. Parrinello, Efficient reconstruction of complex free energy landscapes by multiple walkers metadynamics, J. Phys. Chem. B 110 (2006) 3533–3539.
[42] P. Tiwary, M. Parrinello, A time-independent free energy estimator for metadynamics, J. Phys. Chem. B 119 (2015) 736–742.
[43] J.C. Phillips, R. Braun, W. Wang, J. Gumbart, E. Taj-khorshid, E. Villa, C. Chipot, R.D. Skeel, L. Kalé, K. Schulten, Scalable molecular dynamics with NAMD, J. Comput. Chem. 26 (2005) 1781–1802.
[44] V. Hornak, R. Abel, A. Okur, B. Strockbine, A. Roitberg, C. Simmerling, Comparison of multiple Amber force fields and development of improved protein backbone parameters, Proteins 65 (2006) 712–725.
[45] J.B. Klauda, R.m. Venable, J.A. Freites, J.W. O'Connor, D.J. Tobias, C. Mondragon-Ramirez, I. Vorobyov, A.D. MacKerell Jr., R.W. Pastor, Update of the CHARMM all-atom additive force field for lipids: validation on six lipid types, J. Phys. Chem. B 114 (2010) 7830–7843.
[46] W.L. Jorgensen, J. Chandrasekhar, J.D. Madura, R.W. Impey, M.L. Klein, Comparison of simple potential functions for simulating liquid water, J. Chem. Phys. 79 (1983) 926–935.
[47] K.L. Meagher, L.T. Redman, H.A. Carlson, Development of polyphosphate parameters for use with the AMBER force field, J. Comput. Chem. 24 (2003) 1016–1025.
[48] M. Bonomi, D. Branduardi, G. Bussi, C. Camilloni, D. Provasi, P. Raiteri, D. Donadio, F. Marinelli, F. Pietrucci, R.A. Broglia, M. Parrinello, PLUMED: a portable plugin for free-energy calculations with molecular dynamics, Comput. Phys. Commun. 180 (2009) 1961–1972.
[49] T. Darden, D. York, L. Pedersen, Particle Mesh Ewald-an N.Log(N) method for Ewald sums in large systems, J. Chem. Phys. 98 (1993) 10089–10092.
[50] S. Miyamoto, P.A. Kollman, Settle: an analytical version of the SHAKE and RATTLE algorithm for rigid water models, J. Comput. Chem. 13 (1992) 952–962.
[51] J. Mifsud J, S. Ravaud, E. M. Krammer, C. Chipot, E. R. Kunji, E. Pebay-Peyroula, F. Dehez, The substrate specificity of the human ADP/ATP carrier AAC1, Mol. Membr. Biol. 30 (2013) 160–168.